2012

XRD, AFM, IR and TGA study of nanostructured hydroxyapatite

Mat. Res.,v.15,n.4,p.622-627,2012
http://www.producao.usp.br/handle/BDPI/39846

Materials Research. 2012; 15(4): 622-627
DOI: 10.1590/S1516-14392012005000069

XRD, AFM, IR and TGA Study of Nanostructured Hydroxyapatite

***Mirta Mir*[a], *Fabio Lima Leite*[b]*, *Paulo Sérgio de Paula Herrmann Junior*[c], *Fabio Luiz Pissetti*[a], *Alexandre Malta Rossi*[d], *Elizabeth Lima Moreira*[d], *Yvonne Primerano Mascarenhas*[e]**

[a]*Institute of Exact Science, Federal University of Alfenas – UNIFAL, CEP 37130-000, Alfenas, MG, Brazil*
[b]*Department of Physics, Chemistry and Mathematics, Federal University of São Carlos – UFSCar, CEP 18052-780, Sorocaba, SP, Brazil*
[c]*Alan G. MacDiarmid Institute for Innovation and Business, National Nanotechnology Laboratory for Agribusiness – LNNA, Embrapa Agricultural Instrumentation, São Carlos, SP, Brazil*
[d]*Brazilian Center for Physics Research – CBPF, Urca, RJ, Brazil*
[e]*Department of Physics and Informatics, Physics Institute of São Carlos, University of São Paulo – USP, São Carlos, SP, Brazil*

Received: March 29, 2012; Revised: May 05, 2012

In this work, the synthetic hydroxyapatite (HAP) was studied using different preparation routes to decrease the crystal size and to study the temperature effect on the HAP nano-sized hydroxyapatite crystallization. X-ray diffraction (XRD) analysis indicated that all samples were composed by crystalline and amorphous phases . The sample with greater quantity of amorphous phase (40% of total mass) was studied. The nano-sized hydroxyapatite powder was heated and studied at 300, 500, 700, 900 and 1150 °C. All samples were characterized by XRD and their XRD patterns refined using the Rietveld method. The crystallites presented an anisotropic form, being larger in the [001] direction. It was observed that the crystallite size increased continuously with the heating temperature and the eccentricity of the ellipsoidal shape changed from 2.75 at 300 °C to 1.94, 1.43, 1.04 and 1.00 respectively at 500, 700, 900 and 1150 °C. In order to better characterize the morphology of the HAP the samples were also examined using atomic force microscopy (AFM), infrared spectrometry (IR) and thermogravimetric analysis (TGA).

Keywords: *nanocrystals, AFM, XRD, hydroxyapatite, Rietveld, TGA e IR*

1. Introduction

The hydroxyapatite (HAP), $Ca_{10}(PO_4)_6(OH)_2$, is one of most important bioceramics for hard tissue reconstruction. This application is due to the similarity of the composition of this material with that of the mineral part of bone and tooth[1,2]. The natural bone model presents a combination of organic and inorganic phases with nanometer size (an average length of 50 nm and 25 nm in width)[3]. The small size of the apatite crystalite is a very important factor related with the biological and structural properties such as surface activity, dissolution rate, molding and sintering behavior[4-7]. In order to obtain nanoapatites out of the biological environment and similar to the one in bone, is very important to study how their properties change with the dimensions. In the last years great efforts have been made to produce HAP with low crystal dimensions[4-6]. In some of these studies composites containing HAP and organic molecules have been precipitated in experimental conditions in which the HAP crystals achieved dimensions close to those of bone apatite[8]. Despite many years of experimental synthesis, characterization, and increasing use in applications, many doubts still remain concerning the structure and formation of these nano-crystals. In this work, the synthetic hydroxyapatite (HAP) was prepared using several drying routes to decrease the crystal size and the temperature effect on the HAP nano-sized hydroxyapatite crystallization was studied. X-ray diffraction (XRD) and atomic force microscopy (AFM) were used in order to characterize the nano-sized powder and the powder after thermal treatments. The combination of results obtained from Rietveld refinements of XRD patterns, AFM analysis, infrared spectrometry (IR) and thermogravimetric analysis (TGA) permit a detailed description of changes on particle morphology and particle size with the increase of temperature.

*e-mail: fabioleite@ufscar.br

2. Experimental

2.1. *Materials preparation*

The hydroxyapatite powder were prepared by dropwise addition of calcium nitrate to the ammonium phosphate solution under controlled conditions of temperature, pH, stirring velocity, reagent concentration, addition rate and aging time. The precipitate was separated by filtration, repeatedly washed with deionized water and dried at 37 °C (sample 37c) or lyophilized for 8 or 69 hours (samples

ly8h and ly69h respectively). The synthesis procedure was adjusted in order to produce materials with very small particle size. To study the effect of temperature on crystallization the 69 hours lyophilized sample was heated at 300, 500, 700, 900 and 1150 °C (samples 300c, 500c, 700c, 900c and 1150c, respectively)

2.2. *X-ray diffraction and rietveld refinement*

The X-ray powder diffraction patterns were collected with a Rigaku Rota-flex, using a flat-plate Bragg-Brentano geometry, and graphite monochromated CuKα radiation. The powder diffraction patterns were recorded in the range of 20 – 90°, with a step of 0.02° at 5 second/step. Structural refinement was performed using the Rietveld method as implemented in the computer program package FullProf-Suite[9]. The HAP parameters given by Kay et al.[10] were employed as an initial model for crystal structure refinement. The lanthanum hexaboride (LaB6) standard material was used to model the instrumental resolution. The extraction of the crystallite size and microstrain components of the intrinsic diffraction profile was carried out with the Rietveld method of whole-pattern-fitting structure-refinement. The microstructural effects are treated using the TCH pseudo-Voigt profile function[11]. The intrinsic profile of a particular reflection due to size effect has an integral breadth β_s, from the Scherrer formula $\langle D \rangle = \lambda / (\beta_s \cos \theta)$ provides the volume averaged apparent size of the crystallites in the direction normal to the scattering planes. If the instrumental resolution function is provided after refinement, the program Fullprof calculates the apparent size (in angstrom) along each reciprocal lattice vectors. To obtained the anisotropic size, the spherical harmonics model was using. The intrinsic profile of a particular reflection due to a strain effect has an integral breadth β_d, the apparent strain is defined as $\eta = \beta_d \cot(\theta)$[12]. To conclude if the model is consistent with our data, or to select the best refinement, for each model the R_{wp} (weighted profile agreement factor) was calculated to obtain the probability of correcteness of each model, as suggested by Hamilton[13]. In all cases, except for 1150c, the atomic positions were refined. In the samples *ly8h*, *ly69h*, and 37c the best model was obtained refining the water occupation in the structure. The Table 1 shows the agreement factor between observed and calculated profiles obtained from Rielveld refinement for each sample.

3. Atomic force microscopy (AFM)

In order to compare with the XRD results, particle size and morphology were analyzed using atomic force microscopy (AFM). All measurements were carried out on a Topometrix TMX 2010 Discoverer AFM, operating in contact mode. The cantilevers have a spring constant k = 0.03 Nm^{-1} and tip curvature radius R = 235 nm (MicroleversTM -Veeco Metrology Group). The values of length, width and thickness of the cantilever and the tip radius were measured with a Philips model XL30-FEG SEM. The cantilever elastic constant was calculated using the equation used by Leite et al.[14]. The AFM images were analyzed using WSXM (Nanotec Electronica S.L.) software[15]. The samples were prepared using the layer-by-layer technique[16,17], where HAP particles are deposited onto mica muscovite substrates. The solution of HAP was prepared in deionized water at a concentration of 1 gL^{-1} under continuous stirring for 6 hours. The films were produced by immersion of the substrate into solution for 3 minutes for each layer and after to deposition the plates were dried in a desiccator for 24 hours. The presence of aggregates on the surface was a common characteristic irrespective of the type of substrate and deposition. The size of the particles were determined from the AFM images, after correcting for the effect due to the similar sizes of the tip and particles using the geometric relation described in the literature[18,19].

3.1. *Fourier transform Infrared spectrometry (FTIR) and Thermogravimetric analysis (TGA)*

FTIR spectra of the materials were obtained as pressed KBr pellets, with 4 cm^{-1} of resolution, on a Shimadzu IR Prestige 21 spectrophotometer. Thermogravimetric analyses were carried out on an Instruments Thermoanalyzer, model SDTQ600. The measurements were performed under a flowing nitrogen atmosphere, with a heating rate of 10 °C/min in the range from 30 to 1200 °C.

4. Results and Discussion

The Rietveld refinements of XRD patterns showed that lyophilized samples are formed with greater amounts of amorphous phase (~20% and 40% for 8 and 69 hours of lyophilization, respectively) as compared with ones dried at 37 °C (10% in the sample 37c) (see Figure 1). From Figure 1 and 2 one infers that crystalline phase of sample lyophilized for 8 hours had smaller average apparent crystallite sizes (68 Å), larger strain (39.49[0.044]) the number in brakets is measure the degree of anisotropy) and larger unit cell volume (529.37(4) $Å^3$) than sample lyophilized for 69 hours or dried at 37 °C (see Figure 2). It seems that crystallization water was removed from the HAP structure upon drying, thus decreasing the unit cell volume and the strain while the crystallite mean size increased (see Figures 1 and 2). Since the sample lyophilized for 69 hours exhibited larger amounts of amorphous phase, it was selected to study the effect from the temperature on the crystallization. The drying procedure also affected the structural water present in the sample; in sample lyophilized for 8 hours (*ly8h*) the water occupies 81% of the site (Wyckoff site: 4*e*), the lyophilized for 69 hours (*ly69h*), 71% and in the dried at 37 °C (37c), 100%.

Table 1. The agreement factor (R_{Bragg} and R_{wp}) between observed and calculated profiles obtained from Rietveld refinement.

Sample	*ly8h*	*ly69h*	*37c*	*300c*	*500c*	*700c*	*900c*	*1150c*
R_{Bragg} (%)	1.59	3.39	2.07	2.90	2.27	3.53	3.30	3.82
R_{wp} (%)	4.19	4.59	4.36	5.74	4.89	5.58	5.74	11.2

Figure 3 shows that crystallites presented an anisotropic form, being longer in the [001] direction. With the rise of annealing temperature, the crystallites size increased and the strain decreased to zero at 1150 °C as shown in Figure 1. The sample lyophilized for 69 hours (*ly69h*), which had large amount of amorphous phase, exhibited greater deformation in the tetrahedron where the distance among the atoms P – O2 is greater that P – O1 and P – O3 and the distance among P – Ca1 is also greatest (see Table 2). The sample *ly69h* presents the greatest amount of amorphous phase and deformation of the phosphate tetrahedra in the crystalline phase. Nevertheless, its crystalline phase remained more isotropic compared with the samples and 37c and ly8h. At

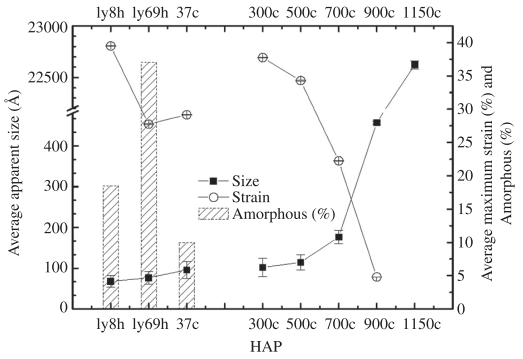

Figure 1. Visualization of the average apparent size (A), average maximum strain (%), and % of amorphous phase obtained from Rietveld refinement for a) ly8h, b) ly69h, c 37c, d) 300c, e) 500c, f) 700c, g) 900c and h) 1150c. The left hand axes correspond to average apparent size (isotropy) and the right hand axis correspond to average maximum strain whith the corresponding standard deviation (anisotropy) and the % of amorphous phase obtained for each sample.

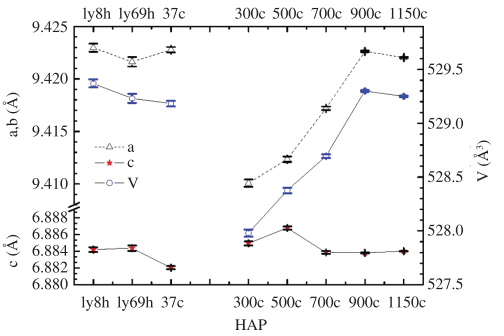

Figure 2. The lattice dimensions and volume of HAP samples determined by the Rietveld refinement with the corresponding error.

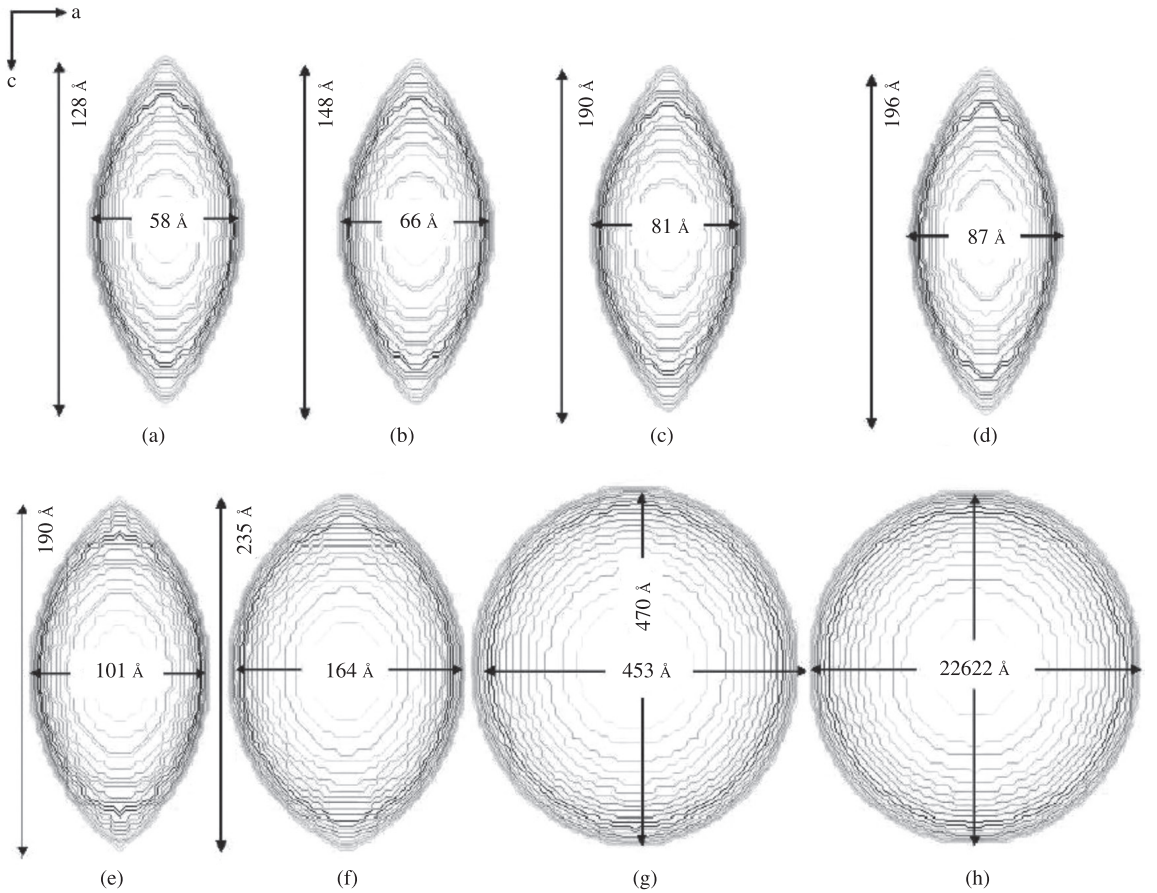

Figure 3. Visualization of the average crystallite shape and size obtained from Rietveld refinement for a) *ly8h*, b) *ly69h*, c) 37c, d) 300c, e) 500c, f) 700c, g) 900c and h) 1150c. The cristalites are greater in the direction of the axis c, presenting an isotropic behavior in a and b axis.

300 °C (sample 300c) where great part of the water in the sample leaves and the volume decreases considerably, the phosphate tetrahedron deformations are smaller and the distances between P – Ca1 are also smaller.

The AFM images of the surface topography of HAP particles deposited on a mica substrate in figure 4 point to an increased particle size for increasing temperatures (300, 500, 700, 900 and 1150 °C). Aggregates on the surface appeared for all samples. The size of the particles was determined from the AFM images. The nanoparticles were anisotropic with ellipsoidal geometry (Figure 3 and 4) with size varying between 220 and 23000 Å for the sample lyophilized for 69 hours and the one sintered at 1150 °C, respectively, in agreement with the values obtained by XRD (see Table 3).

The FTIR spectrum of HAP samples 37c, 300c and 500c presents a broader phosphate band in the 1000 cm^{-1} region

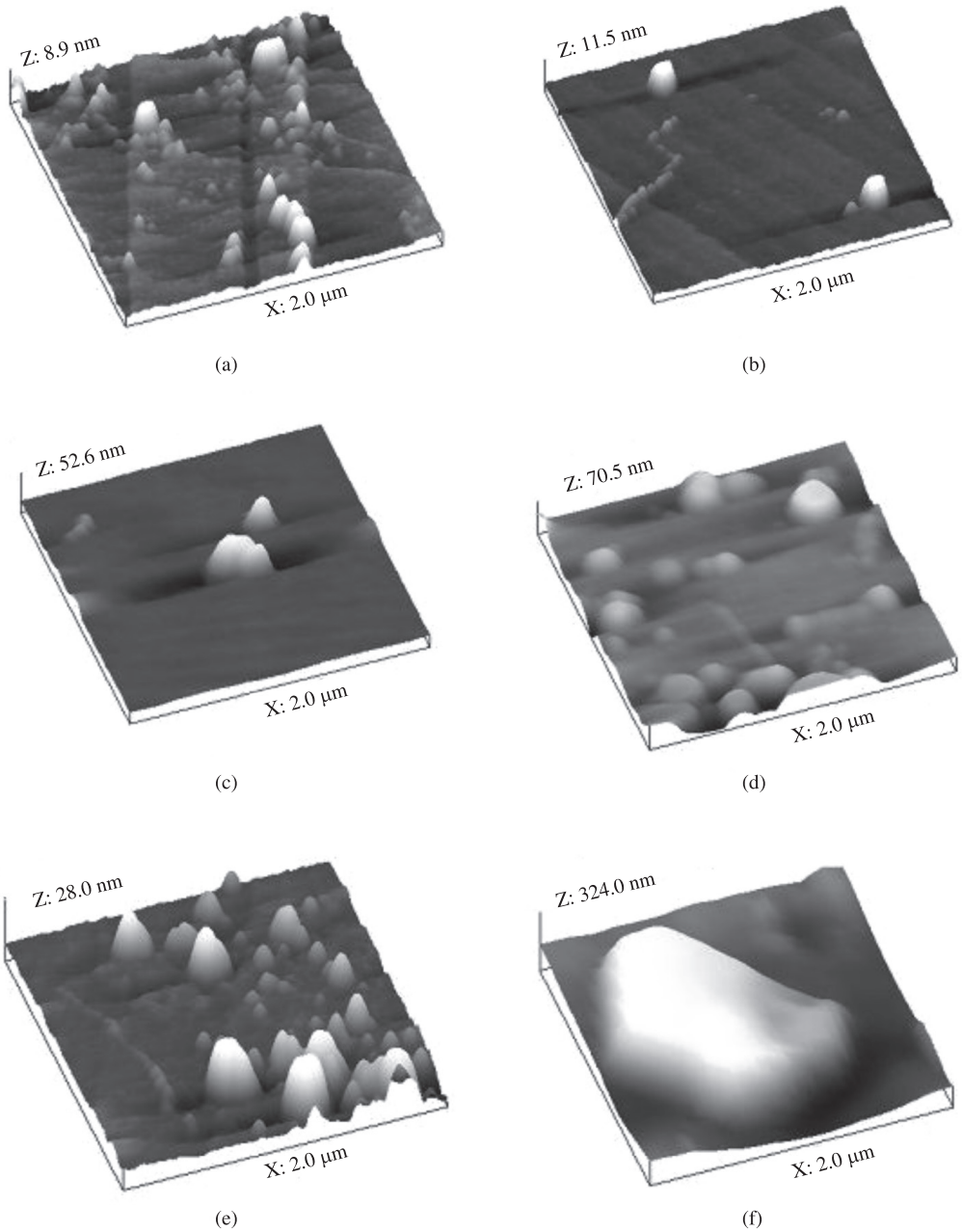

Figure 4. AFM topography of HAP particles deposited on mica by self-assembly by 3 minutes. a) 37c, b) 300c, c) 500c, d) 700c, e) 900c and f) 1150c.

and the absence of OH^- bands at 3570 cm^{-1} and 631 cm^{-1} (see Figure 5). These results are typical of nanocrystalline HAP. For samples 700c, 900c and 1150c the band for PO_4^{3-} vibrational modes become better defined and the OH^- bands are observed, as consequence of the increase in particle size. The incorporation of impurities into the HAP structure probably perturbs the OH^- and PO_4^{3-} vibrational modes. As reported[20], the small crystal size on the nanocrystalline HAP presents a more effective incorporation of CO_3^{2-} and H_2O groups into PO_4^{-3} sites. The FTIR for HAP samples 700c,

Table 2. Interatomic distances of the most nearby neighbors for the crystallographic site and standard deviations obtained from the refinement (in Å).

Distance	Samples							
(neighbors)	*ly8h*	*ly69h*	**37*c***	**300*c***	**500*c***	**700*c***	**900*c***	**1150*c*†**
P-01	1.5316(63)	1.5391(80)	1.5437(53)	1.5696(65)	1.5592(51)	1.5611(48)	1.5602(38)	1.5359
P-02	1.5605(69)	1.6035(88)	1.5579(55)	1.5680(70)	1.5625(54)	1.5614(50)	1.5429(41)	1.5456
(P-03)x2 ‡*a*	1.5182(31)	1.5407(42)	1.5358(27)	1.5599(33)	1.5358(26)	1.5488(25)	1.5571(21)	1.5287
(P-Ca1)	3.1889(32)	3.2120(43)	3.1994(28)	3.1884(35)	3.1985(27)	3.1958(25)	3.2110(19)	3.2144
(P-Ca2)	3.1521(34)	3.1097(46)	3.1176(29)	3.1362(36)	3.1183(28)	3.0982(26)	3.0851(20)	3.0794
(Ca1-01)x3 ‡*b*	2.4025(42)	2.3884(55)	2.3948(36)	2.3827(44)	2.3817(35)	2.3972(33)	3.3932(25)	2.4067
(Ca1-02)x3 ‡*c*	2.4211(40)	2.4054(64)	2.4416(41)	2.4148(51)	2.4322(40)	2.4326(37)	2.4611(30)	2.4534
(Ca1-03)x3 ‡*d*	2.7531(37)	2.7724(47)	2.7849(31)	2.7550(37)	2.7665(29)	2.7763(27)	2.8071(23)	2.8049
Ca2-01	2.7340(54)	2.7342(70)	2.7271(46)	2.6862(57)	2.7106(44)	2.6895(42)	2.6902(32)	2.7051
Ca2-02	2.3797(67)	2.3722(85)	2.3599(54)	2.3597(68)	2.3580(52)	2.3479(49)	2.3435(40)	2.3558
(Ca2-03)x2 ‡*e*	2.5941(40)	2.5139(52)	2.5484(34)	2.5657(41)	2.5531(32)	2.5423(30)	2.5197(25)	2.5117
(Ca2-03)x2 ‡*f*	2.3472(28)	2.3583(37)	2.3368(24)	2.3206(29)	2.3411(23)	2.3245(23)	2.3183(20)	2.3463
(Ca2-OH)x2 ‡*g*	2.4063(35)	2.3690(49)	2.3967(25)	2.4207(32)	2.4030(25)	2.3999(23)	2.3975(19)	2.3809

†Correspond to atomic positions calculated in the paper employed as an initial model[5]. In this sample (1150c) the atomic positions were not refined. ‡ Lengths repeated by symmetry. *a* O: *x, y,* $\bar{z}$ + 1/2; *b* O: $\bar{y}$, 1 + ($\bar{x}$ + *y*), *z* + 1/2; 1 + ($\bar{x}$ + *y*), 1 + ($\bar{x}$), *z*; *c* O: $\bar{y}$, *x* – *y*, – 1 + *z; x* – *y*, 1 + *x, z* – 1/2; 1 + ($\bar{x}$), 1 + ($\bar{y}$), *z* – 1/2; *d* O: *x* – *y*, 1 + *x*, $\bar{z}$; $\bar{y}$, *x* – *y*, $\bar{z}$ + 1/2; 1 + ($\bar{x}$), 1 + ($\bar{y}$), $\bar{z}$; *e* O: *x* – *y*, 1+ *x, z* + 1/2; *x* – *y*, 1 + *x*, $\bar{z}$; *f* O: *x*, 1 + *y, z*; *x*, 1 + *y*, $\bar{z}$ + 1/2; *g* OH: *x*, 1 + *y*, *z*; *y*, 1 + ($\bar{x}$ + *y*), $\bar{z}$.

Table 3. The corrected length (R_p: radius of particle) calculated from the AFM topographic images for two different magnification and the average apparent crystallite sizes obtained by XRD.

Temperature (°C)	AFM		XRD
	***Rp*(Å) (aggregates) (10 × 10 μm)**	***Rp*(Å) (single) (2 × 2 μm)**	**Average apparent size (Å)**
37	220< *Rp* <4500	220 ± 70	81 × 190
300	200< *Rp* <3400	240 ± 40	87 × 96
500	200< *Rp* <300	253 ± 100	101 × 190
700	300< *Rp* <500	450 ± 220	164 × 235
900	350< *Rp* <6000	600 ± 210	453 × 470
1150	8000< *Rp* <23000	1500 ± 5000	22622 × 22622

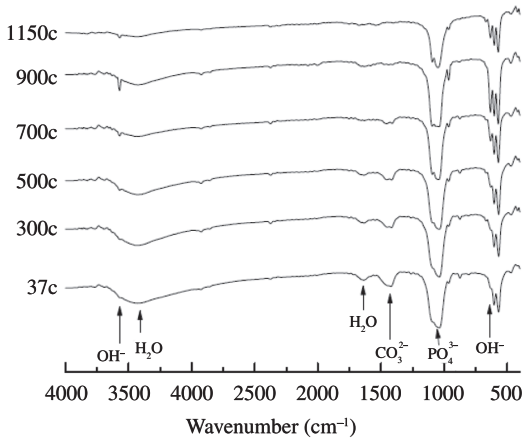

Figure 5. FTIR spectrum of HAP samples. 37c sample corresponds with nano-crystal size.

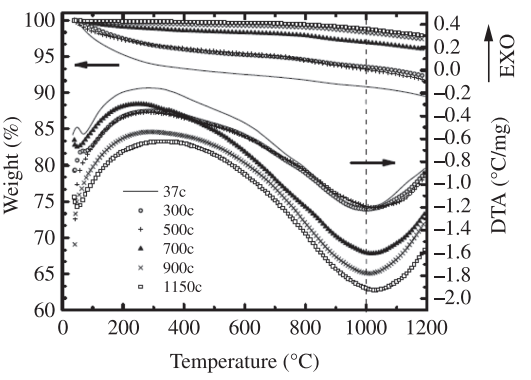

Figure 6. The data of differential thermal analysis (DTA) obtained for the HAP samples. 37c: corresponding to the nano size HAP without heat treatment.

900c and 1150c show a decrease in the bands of these species indicating a higher particle size. The results obtained are consistent with the X-ray and atomic force microscopy data. The data of differential thermal analysis (DTA) for the HAP samples obtained in several temperatures are shown in Figure 6. Here we can see that the HAP decomposition is affected due to the sample presenting smaller crystal sizes. The samples 300c and 500c show a similar behavior to the 37c sample. On the other hand, in the other samples with larger crystal sizes the peak appears after 1000 °C.

5. Conclusion

It was shown that the drying procedure influences the quantity of amorphous phase and crystal size. The samples lyophilized for 69 hours presented the larger amount of amorphous phase. Analysis of the surface topography shows that the size of particles increased with the temperature in agreement with XRD results from the apparent average crystallite sizes. The AFM showed that the particles present an anisotropic form similar to obtained by XRD, where the crystallites are longer in the [001] direction and the eccentricity of the ellipsoidal shape changes from 2.75 at 300 °C to 1.94, 1.43, 1.04 and 1.00 respectively at 500, 700,900 and 1150 °C. The largest particle size was of the order of 23000 Å, estimated from the sample sintered at 1150 °C.

Acknowledgements

The authors gratefully acknowledge the financial support provided by CNPq, FAPEMIG, FAPESP and to Embrapa for the facilities support.

References

1. Kim SY. Surface-engineered hydroxyapatite nanocrystal/ poly (ε-caprolactone) hybrid scaffolds for bone tissue engineering. *Journal of Applied Polymer Science*. 2011; 121:1921-1929. http://dx.doi.org/10.1002/app.33749
2. Zhou H and Lee J. Nanoscale hydroxyapatite particles for bone tissue engineering. *Acta Biomaterialia*. 2011; 7:2769-2781. PMid:21440094. http://dx.doi.org/10.1016/j.actbio.2011.03.019
3. Vallet-Reg M. Evolution of bioceramics within the field of biomaterials. *Comptes Rendus Chimie*. 2010; 13:174-185.
4. Rey C, Combes C, Drouet C, Sfihi H and Barroug A. Physico-chemical properties of nanocrystalline apatites: implications for biominerals and biomaterials. *Materials Science and Engineering*: C. 2007; C27:198-205. http://dx.doi.org/10.1016/j.msec.2006.05.015
5. Kim S, Ryu HS, Shin H, Jung HS and Hong KS. Insitu observation of hydroxyapatite nanocrystal formation from amorphous calcium phosphate in calcium-rich solutions. *Materials Chemistry and Physics*. 2005; 91:500-506. http://dx.doi.org/10.1016/j.matchemphys.2004.12.016
6. Wang F, Li MS, Lu YP, Qi YX and Liu YX. Synthesis and microstructure of hydroxyapatite nanofibers synthesized at 37 °C. *Materials Chemistry and Physics*. 2006; 95:145-149. http://dx.doi.org/10.1016/j.matchemphys.2005.05.034
7. Shen SC, Chia L, Ng WK, Dong YC and Tan RBH. Solid-phase steam-assisted synthesis of hydroxyapatite nanorods and nanoparticles. *Journal of Materials Science*. 2010; 45:6059-6067. http://dx.doi.org/10.1007/s10853-010-4691-1
8. Roveri N, Falini G, Sidoti M.C, Tampieri A, Landi E, Sandri M et al. Biologically inspired growth of hydroxyapatite nanocrystals inside self-assembled collagen fibers. *Materials Science and Engineering*: C. 2003; 23:441-446. http://dx.doi.org/10.1016/S0928-4931(02)00318-1
9. Rodríguez-Caravajal J. *Guide to Program FULPROF for Rietveld Analysis of X-Ray and NeutronPowder Diffraction Patterns with a 'PC' and various other computers*. Laboratoire Leon Brillouin; 2001.
10. Kay MI, Young RA and Posner AS. Crystal structure of hydroxyapatite. *Nature*. 1964; 204:1050-1052. PMid:14243377. http://dx.doi.org/10.1038/2041050a0
11. Thompson P, Cox D and Hastings J. Rielveld refinement of Debye-Scherrer synchrotron x-ray data from Al_2O_3. *JAC - International Union of Crystallography*. 1987; 20:79(83).
12. Stokes AR and Wilson AJC. The diffraction of X-rays by distorted crystal aggregates – I. *Proceedings of the Physical Society*. 1944; 56:174. http://dx.doi.org/10.1088/0959-5309/56/3/303
13. Hamilton WC. Neutron diffraction investigation of the 119 K transition in magnetite. *Physical Review*. 1958; 110:1050-1057. http://dx.doi.org/10.1103/PhysRev.110.1050
14. Leite FL, Riul JA and Herrmann PSP. Mapping of adhesion forces on soil minerals in air and water by Atomic Force Spectroscopy (AFS). *Journal of Adhesion Science and Technology*. 2003; 17:2141-2156. http://dx.doi.org/10.1163/156856103772150751
15. Horcas I, Fernandez R, Gomez-Rodríguez JM, Colchero J, Herrero JG and Baro AM. WSXM: A software for scanning probe microscopy and a tool for nano technology. *Review of Scientific Instruments*. 2007; 78:013705-1-013705-8. PMid:17503926. http://dx.doi.org/10.1063/1.2432410
16. Decher G, Hong J and Schmitt J. Buildup of ultrathin multilayer films by a self-assembly process .3. Consecutively alternating adsorption of anionic and cationic polyelectrolytes on charged surfaces. *Thin Solid Films*. 1992; 210-211:831-835. http://dx.doi.org/10.1016/0040-6090(92)90417-A
17. Leite FL, Paterno LG, Borato CE, Herrmann PSP,Oliveira Junior ON and Mattoso LHC. Study on the adsorption of poly (*o*-ethoxyaniline) nanostructured films using atomic force microscopy. *Polymer*. 2005; 46:12503-12510. http://dx.doi.org/10.1016/j.polymer.2005.07.108
18. Bushell G, Watson G, Holt S and Myhra S. Imaging and nano-dissection of TMV by atomic force microscopy. *Journal of Microscopy*. 1995; 180:174-181. http://dx.doi.org/10.1111/j.1365-2818.1995.tb03673.x
19. Leite FL, De Oliveira Neto M, Paterno LG, Ballestero MR, Polikarpov I, Mascarenhas YP et al. Nanoscale conformational ordering in polyanilines investigated by saxs and afm. *Journal of Colloid and Interface Science*. 2007; 316:376-387. PMid:17905261. http://dx.doi.org/10.1016/j.jcis.2007.08.069
20. Rossi AM, Da Silva MHP, Ramirez DBAJ, Mir M, Mascarenhas YP, Eon JG et al. Structural properties of hydroxyapatite with particle size less than 10 nanometers. *Key Engineering Materials*. 2007; 330-332:255-258. http://dx.doi.org/10.4028/www.scientific.net/KEM.330-332.255